TU Delft

Delft University of Technology

Document Version
Final published version

Licence
CC BY

Citation (APA)
Khadijeh, M., Stüwe, S., Mirwald, J., Hofko, B., Eberhardsteiner, L., & Varveri, A. (2026). Inverse-designed neural networks for rheological prediction of asphalt binders using SARA properties. *International Journal of Pavement Engineering*, *27*(1), Article 2711076. https://doi.org/10.1080/10298436.2026.2711076

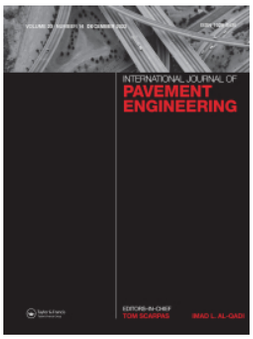
Important note
To cite this publication, please use the final published version (if applicable).
Please check the document version above.

Copyright
In case the licence states “Dutch Copyright Act (Article 25fa)”, this publication was made available Green Open Access via the TU Delft Institutional Repository pursuant to Dutch Copyright Act (Article 25fa, the Taverne amendment). This provision does not affect copyright ownership.
Unless copyright is transferred by contract or statute, it remains with the copyright holder.

Sharing and reuse
Other than for strictly personal use, it is not permitted to download, forward or distribute the text or part of it, without the consent of the author(s) and/or copyright holder(s), unless the work is under an open content license such as Creative Commons.

Takedown policy
Please contact us and provide details if you believe this document breaches copyrights.
We will remove access to the work immediately and investigate your claim.

This work is downloaded from Delft University of Technology.



International Journal of Pavement Engineering

ISSN: 1029-8436 (Print) 1477-268X (Online) Journal homepage: www.tandfonline.com/journals/gpav20

Inverse-designed neural networks for rheological prediction of asphalt binders using SARA properties

Mahmoud Khadijeh, Sophie Stüwe, Johannes Mirwald, Bernhard Hofko, Lukas Eberhardsteiner & Aikaterini Varveri

To cite this article: Mahmoud Khadijeh, Sophie Stüwe, Johannes Mirwald, Bernhard Hofko, Lukas Eberhardsteiner & Aikaterini Varveri (2026) Inverse-designed neural networks for rheological prediction of asphalt binders using SARA properties, International Journal of Pavement Engineering, 27:1, 2711076, DOI: 10.1080/10298436.2026.2711076

To link to this article: https://doi.org/10.1080/10298436.2026.2711076

© 2026 The Author(s). Published by Informa UK Limited, trading as Taylor & Francis Group.

Published online: 02 Aug 2026.

Submit your article to this journal

Article views: 208

View related articles

View Crossmark data

Full Terms & Conditions of access and use can be found at
https://www.tandfonline.com/action/journalInformation?journalCode=gpav20

INTERNATIONAL JOURNAL OF PAVEMENT ENGINEERING
2026, VOL. 27, NO. 1, 2711076
https://doi.org/10.1080/10298436.2026.2711076

Taylor & Francis
by informa

RESEARCH ARTICLE

OPEN ACCESS Check for updates

Inverse-designed neural networks for rheological prediction of asphalt binders using SARA properties

Mahmoud Khadijeh[a], Sophie Stüwe[b], Johannes Mirwald[b], Bernhard Hofko[b], Lukas Eberhardsteiner[c] and Aikaterini Varveri[a]

[a]Department of Engineering Structures, Faculty of Civil Engineering and Geosciences, Delft University of Technology, Delft, Netherlands; [b]Department of Civil and Environmental Engineering, Christian Doppler Laboratory for Chemo-Mechanical Analysis of Bituminous Materials, Institute of Transportation, Research Center of Road Engineering, TU Wien, Vienna, Austria; [c]Department of Civil and Environmental Engineering, Institute of Transportation, Research Center of Road Engineering, TU Wien, Vienna, Austria

ABSTRACT

Asphalt binders, critical for flexible pavement performance, owe their viscoelastic properties to their complex chemical composition, characterised by Saturates, Aromatics, Resins and Asphaltenes (SARA) fractions. This study introduces a bidirectional neural network (BidiNN) framework to predict and optimise the rheological behaviour of asphalt binders based on their SARA composition. The forward model maps chemical inputs, including SARA fractions and environmental conditions, to rheological outputs such as complex modulus (G^*) and phase angle (δ), achieving high accuracy ($R^2 > 0.965$). The inverse model infers optimal SARA fractions to achieve target viscoelastic properties, addressing the non-linear interplay between chemical constituents and mechanical performance. Cycle-consistency losses ensure robust bidirectional predictions, while an ensemble approach captures the non-uniqueness of the inverse problem, generating multiple chemically viable SARA compositions. Chemical characterization separates the binder into SARA fractions. Asphaltenes are first precipitated and removed by filtration, after which the resulting maltene fraction is separated by Solid Phase Extraction (SPE) into saturates, aromatics, and resins.. Aging processes, monitored by Fourier-Transform Infrared (FTIR) spectroscopy, shift SARA distributions toward higher asphaltene content, impacting binder durability. The BidiNN framework enables precise tailoring of chemical compositions for enhanced pavement performance and sustainability.

ARTICLE HISTORY
Received 20 February 2026
Accepted 23 July 2026

KEYWORDS
SARA fractions; asphalt binder; inverse neural network; machine learning; cycle consistent

1 Introduction

1.1 Background on asphalt binders and their importance

Asphalt binders are a critical component in the construction and maintenance of flexible pavements. These materials exhibit viscoelastic properties that are essential for the performance of asphalt mixtures. This viscoelastic behaviour allows asphalt binders to adapt to various environmental conditions, ensuring they perform well under different loading scenarios. The unique properties of asphalt binders stem from their complex chemical composition and structure, making them a significant area of study in materials science and chemical engineering (Khadijeh et al., 2025; Liu & Shan, 2025).

The fundamental understanding of asphalt binder chemistry has evolved substantially in recent decades, moving from empirical characterisation to molecular-level analysis that reveals the relationship between chemical composition and mechanical performance (Pipintakos et al., 2024). This evolution in understanding has coincided with growing environmental and economic pressures to extend pavement lifespans and develop more sustainable practices in road construction and maintenance (Mior Sani et al., 2024). A key approach to characterising the chemical composition of asphalt binders is the SARA fractionation method, which categorises binders into four distinct chemical fractions: Saturates, Aromatics, Resins and

CONTACT Mahmoud Khadijeh m.khadijeh@tudelft.nl
This article has been corrected with minor changes. These changes do not impact the academic content of the article.

© 2026 The Author(s). Published by Informa UK Limited, trading as Taylor & Francis Group.
This is an Open Access article distributed under the terms of the Creative Commons Attribution License (http://creativecommons.org/licenses/by/4.0/), which permits unrestricted use, distribution, and reproduction in any medium, provided the original work is properly cited. The terms on which this article has been published allow the posting of the Accepted Manuscript in a repository by the author(s) or with their consent.

Article highlights

- Bidirectional NN predicts asphalt binder rheology from SARA fractions with high accuracy.
- Cycle-consistent BidiNN enables robust forward and inverse rheological predictions.
- Inverse model optimises SARA fractions for desired viscoelastic properties.
- Total loss combines MSE and cycle-consistency for precise SARA-rheology predictions.

Asphaltenes. This classification, based on polarity and solubility, provides valuable insights into binder performance characteristics under different environmental and mechanical conditions.

To accurately separate and quantify SARA fractions, various analytical techniques have been developed. Traditional methods such as Gravimetric Adsorption Chromatography, as outlined in ASTM D4124, rely on precipitating Asphaltenes using *n*-heptane, followed by chromatographic separation of maltenes into Saturates, Aromatics and Resins using silica and alumina columns. Although widely adopted, these methods can be time-consuming and may lack precision (Karevan et al., 2022).

Latest method developments offer enhanced speed, reproducibility and automation. Solid Phase Extraction (SPE), for instance, simplifies the separation of maltenes by using packed columns (e.g. silica or alumina) and a stepwise solvent gradient to elute Saturates, Aromatics and Resins in sequence after asphaltene precipitation (Schwettmann et al., 2022). SPE provides a more consistent and reproducible alternative to traditional gravimetric methods, with reduced solvent consumption and improved fraction isolation.

Another rapid and reproducible technique is Thin-Layer Chromatography–Flame Ionisation Detection (TLC-FID). The Iatroscan TLC-FID system, for example, can complete an analysis in approximately 30 s, addressing the throughput limitations of older chromatographic methods (Li et al., 2025).

High-Performance Liquid Chromatography (HPLC) also allows precise quantification of SARA fractions using columns with tailored stationary phases. This method offers excellent separation efficiency and reduces both analysis time and solvent use compared to conventional methods (Kheirollahi et al., 2024). Considering separation into fractions, the SARA components follow a general increase in molar mass, aromaticity and relative molecular polarity from saturates to asphaltenes. Saturates are the least polar, consisting mainly of aliphatic hydrocarbons with minimal aromaticity. Aromatics (sometimes referred to as naphthene aromatics) contain unsaturated aromatic ring systems and exhibit slightly higher polarity. Resins, also described as polar aromatics, contain fused aromatic structures and show greater polarity relative to saturates and aromatics. Asphaltenes represent the most polar and highest-molecular-weight fraction, characterised by condensed aromatic ring systems; however, their polarity must be understood as high relative to the other SARA fractions within the generally low-polarity bitumen matrix (Mikhailenko & Baaj, 2019; Petersen, 2009; Read & Whiteoak, 2003).

1.2 Influence of SARA composition on rheological behaviour, aging and rejuvenation of asphalt binders

The rheological properties of asphalt binders, including viscosity, stiffness and viscoelastic behaviour, are closely related to their SARA composition. Each fraction plays a distinct role in determining the performance of binder under varying temperatures, loading conditions and aging processes, which makes this relationship essential for optimising pavement durability and sustainability, particularly with the use of rejuvenators (Mansourkhaki et al., 2020).

Saturates, being non-polar aliphatic hydrocarbons, reduce viscosity and enhance low temperature flexibility, improving workability during mixing and compaction, though excessive Saturates may lead to rutting at high temperatures. Aromatics, slightly polar with oily consistency, improve ductility and fatigue resistance, maintaining viscoelastic balance for recovery from cyclic loading. Resins, polar and high-molecular-weight, stabilise Asphaltenes within the maltene phase, enhancing adhesion and elasticity, with the resin-to-asphaltene ratio serving as a key indicator of the stability of the binder (Ashoori et al., 2017). Asphaltenes, the most polar and complex fraction, increase stiffness and viscosity, improving rutting resistance but potentially causing brittleness if overly abundant (Shi et al., 2017). A balanced

SARA composition ensures a stable colloidal structure, while an imbalance, such as high Asphaltenes with insufficient Resins, can lead to cracking (Ma et al., 2023; Wang et al., 2019).

Aging, driven by oxidative processes and various environmental factors, indicates a shift toward higher polar fractions (namely resins and asphaltenes). This shift is linked with an increase in carbonyls and sulfoxides results in an increase in stiffness and elasticity of the binder, which is thought to improve the rutting resistance, but comprises low-temperature performance and fatigue resistance (Jiang et al., 2024; Mirwald et al., 2020). Techniques such as TLC-FID, HPLC and SPE show that aged binders have a higher ratio of Asphaltenes to maltenes. The complex shear modulus (G^*) represents the total resistance of the binder to deformation under oscillatory loading, capturing its overall viscoelastic stiffness. The phase angle (δ) quantifies the lag between applied shear stress and resulting strain, indicating the balance between elastic response (low δ) and viscous flow (high δ). Both parameters are determined using Dynamic Shear Rheometer (DSR) testing according to standardised measurement protocols. This change is linked to an increase in G^* and a decrease in δ, indicating that the binder becomes more elastic but less ductile (Kheirollahi et al., 2024).

To counteract these effects, recycling agents, also referred to as regeneration agents, are commonly used to restore the SARA balance. These agents primarily increase the Aromatic and Resin fractions, enhancing Asphaltene dispersion and improving colloidal stability (Cavalli et al., 2018; Kakar et al., 2019). This results in a softer binder with reduced viscosity and improved resistance to low-temperature cracking, while still maintaining adequate stiffness to resist rutting. Bio-based oils and petroleum derived Aromatic extracts are typical examples of such agents. When evaluated using DSR, these regeneration agents are shown to lower G^* and increase in δ, effectively mimicking the rheological behaviour of virgin binders (Pipintakos et al., 2024). In addition, bio-based regeneration agents significantly reduce the glass transition temperature, thereby enhancing low-temperature performance (Li et al., 2025). These measurements are essential for assessing the impact of aging and the restorative potential of recycling and regeneration agents on binder performance.

Fourier Transform Infrared Spectroscopy (FTIR) identifies chemical changes due to aging or rejuvenation, particularly the formation of carbonyl (C═O) and sulfoxide (S═O) functional groups through oxidation processes. The dominant oxidation reactions involve aliphatic side chains attached to aromatic molecules through a free-radical chain mechanism. During aging, oxygen reacts with these side chains to form hydroperoxide intermediates, which subsequently decompose into carbonyl-containing species and other oxygenated products. This process can be schematically represented as:

$$\mathrm{R{-}CH_2{-}CH_2{-}R' \xrightarrow[\text{oxidation}]{O_2} R{-}CH_2{-}CH(OOH){-}R' \rightarrow C{=}O\text{-containing species.}} \quad (1)$$

This oxidation pathway contributes to the progressive increase in polarity of the maltene phase (Mirwald et al., 2020; Petersen, 2009). The resulting shift toward higher polar fractions—namely resins and asphaltenes—is associated with increased stiffness and elasticity of the binder, which is thought to improve rutting resistance but compromises low-temperature performance and fatigue resistance (Jiang et al., 2024; Mirwald et al., 2020).

The conversion of lighter fractions toward asphaltenic material during aging is a complex, multi-pathway process. Several concurrent mechanisms have been proposed in the literature, including oxidative condensation of resin molecules, aromatisation of naphthenic ring systems, dehydrogenation reactions leading to polycyclic aromatic growth, molecular aggregation and progressive polarity changes within the maltene phase (Jiang et al., 2024; Petersen, 2009). The resin-to-asphaltene conversion therefore represents one of several contributing pathways rather than a single direct transformation. These processes collectively shift the SARA balance toward higher asphaltene content, resulting in an increase in G^* and a decrease in δ, indicating that the binder becomes more elastic but less ductile (Kheirollahi et al., 2024).

Table 1 summarises the distinct rheological roles of each SARA fraction, their transformations due to aging, and the corresponding effects of rejuvenators in restoring binder performance.

1.3 Optimising asphalt binder properties with inverse neural networks

The accurate prediction of the rheological behaviour of asphalt binders based on their chemical composition presents significant challenges. The complex non-linear relationships between these chemical constituents and the

Table 1. Influence of SARA fractions on rheological properties and rejuvenator effects.

Fraction	Rheological contribution	Impact of aging	Rejuvenator effect
Saturates	Reduces viscosity, enhances low-temperature flexibility	Minimal change	Slightly increased to improve workability
Aromatics	Improves ductility, fatigue resistance	Reduced due to oxidation	Replenished to restore flexibility
Resins	Enhances adhesion, elasticity	Reduced through oxidation, condensation and aggregation processes; contributes to asphaltene growth as one of several aging mechanisms	Increased to stabilise Asphaltenes
Asphaltenes	Increases stiffness, rutting resistance	Increased, causing brittleness	Dispersed to reduce brittleness

mechanical properties of binders, such as viscosity and stiffness, are influenced by various factors including aging, DSR test parameters and the use of various additives, including regeneration agents. Traditional analytical methods often struggle to capture these intricate interactions, leading to limitations in predicting binder performance under diverse conditions. Recent advancements in machine learning offer promising solutions to these challenges. Inverse neural networks are designed to predict input parameters required to achieve the desired output properties (Genzel & Macdonald, 2022). Unlike conventional neural networks, which map inputs such as SARA fractions and temperature to outputs like rheological properties, inverse neural networks invert this process by estimating the input conditions necessary to obtain specified performance characteristics. During training, the network minimises the error between predicted and actual inputs for given outputs, often incorporating physical constraints to ensure that solutions remain within realistic bounds. Despite their potential, applying inverse neural networks to asphalt binder design presents several challenges. This occurs because multiple compositional configurations can produce nearly identical rheological properties, due to the complex, many-to-one relationship between chemical makeup and mechanical behaviour. This creates an ill-posed inverse problem, where various solutions meet the mathematical criteria but differ in practical application (Kumar et al., 2020).

1.4 Research objectives and paper overview

This study investigates the intricate, non-linear interdependencies between the chemical composition, aging mechanisms and mechanical properties of asphalt binders by employing a bidirectional neural network (BidiNN) framework that incorporates both forward and inverse mappings. The forward model predicts rheological properties based on input variables such as SARA fractions, aging conditions and testing parameters. In contrast, the inverse model infers the necessary chemical composition and aging state required to attain the targeted rheological performance, thereby supporting the custom design of asphalt binders for improved durability and sustainability. To ensure robust learning in both directions, the model is trained with cycle-consistency losses, which enforce consistency between original and reconstructed inputs and outputs across the dual mappings. The approach is applied to a real-world dataset comprising both aged and unaged binders under diverse conditions, providing a comprehensive understanding of the behaviour of asphalt binder and demonstrating the utility of bidirectional learning for performance-driven material optimisation.

2 Experimental measurements

Investigating the relationship between SARA fractions and the rheological properties of asphalt binders required a comprehensive experimental program aimed at generating high-quality data for training and validating the bidirectional neural network. The program consisted of aged and unaged asphalt binder samples tested under standardised laboratory conditions. The experimental workflow was structured around three main components: (1) chemical characterisation of SARA fractions, (2) rheological testing to evaluate viscoelastic behaviour and (3) aging and FTIR Spectroscopy studies to monitor compositional and performance changes.

2.1 Chemical characterisation of SARA fractions

Since bitumen is a complex material, consisting of millions of different molecules, a way to simplify its chemical composition is often sought after. A novel SPE technique was used to achieve this simplification

more efficiently (Sakib & Bhasin, 2019). In this process, approximately 400 ± 20 mg of the binder was dissolved in 40 ml of *n*-heptane and stirred at room temperature for 24 ± 2 h. Asphaltenes were then removed by filtration using four Thermo Scientific™ Titan3™ PTFE syringe filters (25 mm diameter, 0.2 µm pore size). Subsequently, 5 ml of *n*-heptane were added to each of the four maltene solutions. Two of the resulting maltene solutions were then diluted to a concentration of 3.33 mg/ml and loaded onto a Thermo Scientific™ HyperSep™ Silica SPE cartridge (40–63 µm pore size) mounted on a vacuum manifold. After prewashing the cartridge and applying the maltene solution, the remaining three fractions were sequentially eluted using the solvents specified in Table 2.

Following the separation process, the solvent was removed using a heating plate in combination with a continuous stream of nitrogen to minimise oxidation. Portions of the maltenes and the individual SARA fraction solutions were then evaporated under a nitrogen atmosphere and weighed to determine the gravimetric distribution of the maltenes and the respective Saturates, Aromatics and Resins fractions within the binders. The resulting weight was back-calculated to obtained the percentage of the four individual SARA fractions that were used as an input for the neural network. As this process was done twice, the averaged percentages of each SARA fraction was used for analysis (Figure 1).

2.2 Rheological testing

The rheological properties of the material were assessed using an Anton Paar MCR 302 dynamic shear rheometer. For sample preparation, the binders were heated and homogenised at a maximum temperature of 140 °C, then cast into silicone moulds – 8 mm in diameter for lower temperature tests and 25 mm for higher temperature evaluations. The samples were stored in the dark for 24 h prior to testing, following the guidelines of EN 14770. Rheological measurements were conducted across a frequency range of 0.1 to 40 Hz and a temperature range of −30 °C to 82 °C to comprehensively characterise the viscoelastic behaviour of the material.

2.3 Laboratory aging and FTIR spectroscopy

Laboratory short-term aging (STA) was conducted using the Rolling Thin Film Oven Test (RTFOT), which was performed following the EN 12607-1 (163 °C for 75 min). For laboratory long-term aging

Table 2. Overview of the solvents and their respective ratios used for separation (Sakib & Bhasin, 2019).

Fraction	Quantity [ml]	Solvent	Ratio [vol%]
Prewash	20	*n*-Heptane	100
Saturates	10	*n*-Heptane	100
Aromatics	25	Toluene: *n*-Heptane	80:20
Resins	40	Dichloromethane: Methanol	90:10



Figure 1. Visual representation of the SARA fractionation process. Taken and adapted from Mirwald et al. (2020).

(LTA), the Pressure aging Vessel (PAV) test was used, which was performed following the EN 14679 with a pressure of 2.1 MPa, a temperature of 100 °C and an aging duration of 20 h.

To evaluate the impact of these aging processes on the chemical structure of the binders, ATR-FTIR spectroscopy was used to capture the chemical composition of the binders from a perspective of IR active molecular groups such as oxygen containing functional groups including carbonyls and sulphoxides that are often used to evaluate or track aging. For the respective measurement, a Bruker Alpha II spectrometer equipped with an ATR unit featuring a diamond crystal and a deuterated triglycine sulphate (DTGS) detector was utilised. For each binder, a small amount of the material was briefly heated to 140 °C for no more than one minute, in line with recommendations from literature (Mirwald et al., 2022). Once the binder had reached a liquid-like state, four small droplets were placed onto silicone paper after ensuring thorough homogenisation, which was done using a thermometer. After cooling the samples for approximately five minutes, spectra were recorded within the 4000–680 cm^{-1} range, using a resolution of 4 cm^{-1} and 24 scans per measurement. Each of the four binder samples were analysed with four replicates (ensuring device precision), resulting in a total of 16 spectra per binder. For spectral analysis, a min-max normalisation was applied within the 3200–2800 cm^{-1} region, which only captures the aliphatic vibrations that are traditionally not affected by changes of the material. The normalised spectra were then integrated by a full baseline integration using the following spectral regions:

- Carbonyls (AICO): 1660–1800 cm^{-1}
- Sulfoxides (AISO): 1079–984 cm^{-1}
- Polarity Region (AIPol): 1330–1130 cm^{-1}

While the carbonyl and sulphoxide indices are widely recognised as indicators of aging due to their reflection of oxygen incorporation, the polarity region corresponds to an increase in molecular polarity within bitumen. This shift can be evaluated using SARA fractionation, as noted in the literature, which also reports that fractions with higher polarity show significantly greater absorbance in the 1330–1130 cm^{-1} range (Mirwald et al., 2020). As a result, integration over this spectral region can be associated with changes in the SARA fractions, although no quantitative correlation has been established to date.

The respective aging index was then calculated by adding up the resulting values obtained from the integration for the overall AIFTIR. This AI represents the mean value of the area obtained for the respective integral regions of all 16 spectra (Figure 2).

It is important to note that the FTIR data acquired in this work was not used as an input feature for the bidirectional neural network. Only the experimentally determined SARA fractions, together with temperature, frequency and aging condition, were employed in model training and prediction. The FTIR

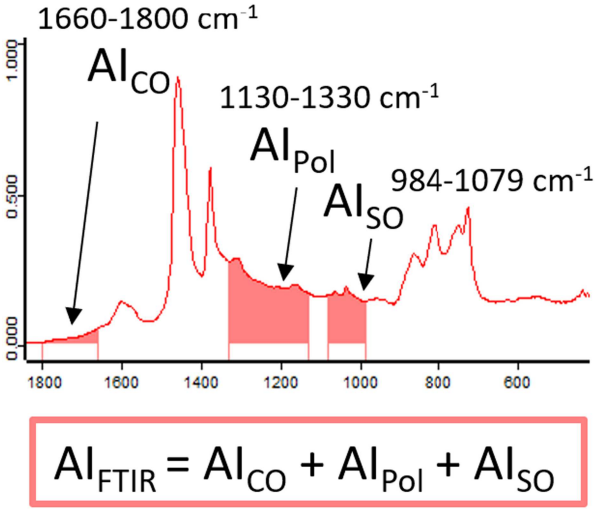


Figure 2. Aging Index derived from ATR-FTIR measurements considering carbonyl, sulphoxide and polarity bands.

measurements serve purely as supporting chemical characterisation, providing independent confirmation that the applied laboratory aging procedures induced the expected oxidative processes, namely the increase in carbonyl, sulfoxide and polarity-related absorbance bands. These spectral changes are well established as indicators of molecular oxidation and increasing polarity in aged binders and therefore help validate the interpretation that shifts in SARA fractions arise from chemical aging rather than measurement noise or separation artifacts. FTIR thus strengthens the experimental foundation of the study while remaining external to the machine-learning framework.

2.4 Dataset description

A comprehensive dataset comprising 5830 data points was compiled from experimental tests on 70 unique asphalt binders. The binders are all unmodified bituminous materials; they vary in crude oil source and refinery origin, which drives the compositional diversity captured in Table 3.

A subset originates from the same crude oil source but was collected at different seasons or production batches, introducing realistic within-source variability. Full provenance information for all binders is not available, as the supplying companies treat crude oil source and refinery conditions as proprietary information, a common constraint in industry-collaborative research on bitumen. The dataset combines samples characterised within the present study with samples from prior independent research projects conducted in the same laboratory at TU Wien, all measured using the identical SPE fractionation and DSR protocols described in Sections 2.1 and 2.2. This pooling of consistently measured data is standard practice in machine learning studies on asphalt materials, where the scarcity of SARA + rheological datasets limits model training.

Each data point corresponds to a single measurement of G^* and δ at one specific (temperature, frequency) combination for one binder in one aging state. DSR testing spans a frequency range of 0.1 to 40Hz and a temperature range of −30 °C to 82 °C (Section 2.2). Not all binders were measured across the full temperature–frequency grid, and not all were subjected to PAV aging; a subset was characterised in the fresh (unaged) condition only. The total of 5830 data points therefore results from summing the individual temperature–frequency measurement counts across all binder–aging-state combinations. Aging conditions were encoded as three continuous physical input variables: aging temperature (°C), aging time (h) and aging pressure (MPa). For fresh (unaged) binders these take values of 0 °C, 0 h and 0 MPa respectively; for PAV long-term aged binders they take values of 100 °C, 20 h and 2.1 MPa. This continuous encoding, rather than a categorical label, allows the model to interpret the physical severity of the aging protocol directly.

This dataset's diversity and scale enable the BidiNN to capture the non-linear interdependencies between chemical composition, environmental conditions and rheological properties, facilitating both forward predictions of viscoelastic behaviour and inverse design of optimal SARA compositions.

3 Neural network design and training

This section outlines the bidirectional neural network framework developed for predicting rheological properties from SARA fractions and designing SARA compositions to achieve target performance. The framework integrates forward and inverse models with cycle-consistency to ensure robust predictions, addressing the complex nonlinear relationships in asphalt binder behaviour.

Table 3. Statistical summary of the experimental dataset for 70 asphalt binders (5830 data points).

Statistic	Asphaltenes (%)	Aromatics (%)	Saturates (%)	Resins (%)	Test temperature (°C)	Test frequency (Hz)
Mean	19.45	46.71	22.18	13.17	48.18	10.59
Std	4.23	5.92	3.71	3.08	24.06	12.79
Min	11.94	34.86	14.23	8.16	−30.00	0.03
Median	19.31	47.94	21.85	13.03	52.00	5.00
Max	28.48	57.69	30.32	19.20	82.00	40.00
Variance	17.93	35.10	13.78	9.51	578.96	163.55

3.1 Model architecture

The BidiNN is designed to model the complex relationship between input features $\mathbf{x} \in \mathbb{R}^{d_x}$ and output responses $\mathbf{y} \in \mathbb{R}^{d_y}$, where $d_x = 9$ represents the nine input features: Asphaltenes content, Naphthene Aromatics content, Saturates content and Resins content (all in wt.%), aging temperature (°C), aging time (h), aging pressure (MPa), test temperature (°C) and test frequency (Hz), and $d_y = 2$ corresponds to the outputs (G^* and δ). The architecture comprises three main components: an encoder, a forward mapping network and an inverse mapping network, enabling both forward (x → y) and inverse (y → x) predictions with cycle-consistency constraints.

The encoder $\mathrm{h} : \mathbb{R}^{d_x} \to \mathbb{R}^{100}$ transforms the input features into a latent representation:

$$\mathrm{h}(x) = \sigma(W_2 \cdot \sigma(W_1 \cdot \mathrm{x} + b_1) + b_2), \tag{2}$$

where $W_1 \in \mathbb{R}^{100 \times d_x}$, $W_2 \in \mathbb{R}^{100 \times 100}$, b_1, $b_2 \in \mathbb{R}^{100}$ are learnable parameters and σ is the hyperbolic tangent (tanh) activation function.

The forward mapping network $\mathrm{f} : \mathbb{R}^{100} \to \mathbb{R}^{d_y}$ predicts the output responses from the latent representation:

$$\mathrm{f}(\mathrm{h}(\mathrm{x})) = W_7 \cdot \sigma(W_6 \cdot \sigma(W_5 \cdot \sigma(W_4 \cdot \sigma(W_3 \cdot \mathrm{h}(\mathrm{x}) + b_3) + b_4) + b_5) + b_6) + b_7, \tag{3}$$

where W_3, W_4, W_5, $W_6 \in \mathbb{R}^{100 \times 100}$, $W_7 \in \mathbb{R}^{d_y \times 100}$ and b_3, b_4, b_5, $b_6 \in \mathbb{R}^{100}$, $b_7 \in \mathbb{R}^{d_y}$. This network consists of six fully connected hidden layers with tanh activations, providing sufficient depth to capture nonlinear relationships.

The inverse mapping network $\mathrm{g} : \mathbb{R}^{d_y} \to \mathbb{R}^{d_x}$ reconstructs the input features from the output responses:

$$\mathrm{g}(\mathrm{y}) = W_{12} \cdot \sigma(W_{11} \cdot \sigma(W_{10} \cdot \sigma(W_9 \cdot \sigma(W_8 \cdot \mathrm{y} + b_8) + b_9) + b_{10}) + b_{11}) + b_{12}, \tag{4}$$

where $W_8 \in \mathbb{R}^{100 \times d_y}$, W_9, W_{10}, $W_{11} \in \mathbb{R}^{100 \times 100}$, $W_{12} \in \mathbb{R}^{d_x \times 100}$ and b_8, b_9, b_{10}, $b_{11} \in \mathbb{R}^{100}$, $b_{12} \in \mathbb{R}^{d_x}$. Similar to the forward network, it uses six layers with tanh activations.

Cycle-consistency is enforced by composing the forward and inverse mappings, ensuring that $\mathrm{g}(\mathrm{f}(x)) \approx x$ and $\mathrm{f}(\mathrm{g}(y)) \approx y$. This bidirectional architecture enhances model robustness and interpretability by learning consistent mappings in both directions.

3.2 Training process

The BidiNN is trained to minimise a composite loss function that balances forward prediction accuracy, inverse reconstruction fidelity and cycle-consistency. The dataset is split into training (80%) and test (20%) sets, with input features and outputs standardised using z-score normalisation. The frequency input and G^* output are log-transformed to handle their wide dynamic ranges:

$$x'_{\mathrm{freq}} = \ln(1 + x_{\mathrm{freq}}), \quad y'_{G^*} = \ln(1 + y_{G^*}), \tag{5}$$

where x_{freq} and y_{G^*} are clipped to a minimum of 10^{-10} to avoid numerical issues.

The loss function comprises four components:

- **Forward loss**: Measures the mean squared error (MSE) between predicted and true outputs:

$$\mathcal{L}_{\mathrm{forward}} = \frac{1}{N} \sum_{i=1}^{N} \|\mathbf{f}(\mathbf{h}(\mathbf{x}_i)) - \mathbf{y}_i\|_2^2, \tag{6}$$

where N is the number of training samples.

- **Inverse loss**: Quantifies the MSE between reconstructed and true inputs:

$$\mathcal{L}_{\text{inverse}} = \frac{1}{N}\sum_{i=1}^{N}\|\mathbf{g}(\mathbf{y}_i) - \mathbf{x}_i\|_2^2. \tag{7}$$

- **Forward cycle-consistency loss**: Ensures that inputs reconstructed through the forward-inverse cycle match the original inputs:

$$\mathcal{L}_{\text{cycle-x}} = \frac{1}{N}\sum_{i=1}^{N}\|\mathbf{g}(\mathbf{f}(\mathbf{h}(\mathbf{x}_i))) - \mathbf{x}_i\|_2^2. \tag{8}$$

- **Inverse cycle-consistency loss**: Ensures that outputs reconstructed through the inverse-forward cycle match the original outputs:

$$\mathcal{L}_{\text{cycle-y}} = \frac{1}{N}\sum_{i=1}^{N}\|\mathbf{f}(\mathbf{h}(\mathbf{g}(\mathbf{y}_i))) - \mathbf{y}_i\|_2^2. \tag{9}$$

The total loss is a weighted sum:

$$\mathcal{L}_{\text{total}} = \mathcal{L}_{\text{forward}} + \mathcal{L}_{\text{inverse}} + \lambda\,(\mathcal{L}_{\text{cycle-x}} + \mathcal{L}_{\text{cycle-y}}), \tag{10}$$

where $\lambda = 1.0$ is the cycle-consistency weight. The model is optimised using the Adam optimiser with a learning rate of 10^{-4} over 5000 epochs, with early stopping based on the test forward loss (patience of 500 epochs). The training process is seeded for reproducibility (seed = 42). Table 4 summarises the all the hyperparameters used in the BidiNN model. The hyperparameters were determined through a structured validation-based selection procedure. Hidden layer size (100 units) and depth (4 layers) were selected after testing smaller and larger configurations. The `tanh` activation was preferred over ReLU for its more stable gradient behaviour in the inverse mapping. A learning rate of 10^{-4} was chosen after 10^{-3} caused oscillations in the cycle-consistency loss. The cycle-consistency weight $\lambda = 1.0$ was selected after testing values between 0.1 and 2.0, providing the best balance between forward prediction accuracy and inverse reconstruction fidelity.

3.3 Validation and performance metrics

Model performance is evaluated on both training and test sets using the coefficient of determination (R^2) for forward, inverse and cycle-consistency predictions. The R^2 score for a predicted variable $\hat{z}$ against true values z is defined as:

Table 4. Hyperparameters used in the BidiNN model.

Parameter	Value	Description
Random seed	42	Fixed seed for reproducibility
Train/test split	80:20	Data partitioning ratio
Learning rate	0.0001	Adam optimiser learning rate
Maximum epochs	5000	Training epoch limit
Early stopping patience	500	Epochs without improvement
Encoder hidden units	100	Shared encoder layer size
Forward network layers	6×100	Hidden layers in forward path
Inverse network layers	6×100	Hidden layers in inverse path
Activation function	Tanh	Non-linear activation
Loss function	MSE	Mean squared error
Cycle consistency weight	1.0	λ parameter for cycle loss
Input dimension	9	Number of input features
Output dimension	2	Number of output features
Normalisation	StandardScaler	Feature scaling method
Loss recording interval	10 epochs	Monitoring frequency

$$R^2 = 1 - \frac{\sum_{i=1}^{N} (z_i - \hat{z}_i)^2}{\sum_{i=1}^{N} (z_i - \bar{z})^2}, \tag{11}$$

where $\bar{z}$ is the mean of the true values.

For forward predictions, R^2 scores are computed for G^* and δ by comparing predicted values $\mathrm{f}(h(\mathrm{x}_i))$ to true outputs $\mathbf{y}_i$, with log transformations reversed for G^*. Inverse predictions are evaluated by comparing reconstructed inputs $\mathrm{g}(\mathrm{y}_i)$ to true inputs x_i, with the frequency feature transformed back to the original scale:

$$x_{\text{freq, recon}} = \exp(x'_{\text{freq, recon}}) - 1. \tag{12}$$

Physical constraints are applied to reconstructed inputs (e.g. non-negative frequency, pressure and composition percentages within [0, 100]). Figure 3 shows the bidirectional neural networks architectures used in this study.

3.4 Ensemble method for multiple solution generation

While the BidiNN successfully generates inverse predictions from rheological properties to material composition and processing conditions, the deterministic nature of the model produces a single solution for each set of input rheological data. However, the inverse problem of determining material composition from rheological properties is inherently non-unique, meaning multiple combinations of composition and processing parameters can yield similar rheological responses. To address this limitation and explore the solution space more comprehensively, an ensemble-based approach was developed to generate multiple physically valid solutions that capture the uncertainty in the inverse mapping.

The ensemble approach leverages model uncertainty by creating multiple variants of the trained bidirectional neural network, each representing a slightly different interpretation of the learned mapping. The methodology begins with the trained base model $\mathcal{M}_{\text{base}}$ with optimised parameters θ_{base}. Multiple ensemble members $\mathcal{M}_k$ are generated by introducing controlled perturbations to the network weights:

$$\theta_k = \theta_{\text{base}} + \epsilon_k, \quad k = 1, 2, \ldots, K, \tag{13}$$

where $\epsilon_k \sim \mathcal{N}(0, \sigma^2 I)$ represents Gaussian noise with standard deviation $\sigma = 0.01$ applied independently to each parameter. The perturbation magnitude is carefully chosen to preserve the learned relationships while introducing sufficient variability to explore different regions of the parameter space.

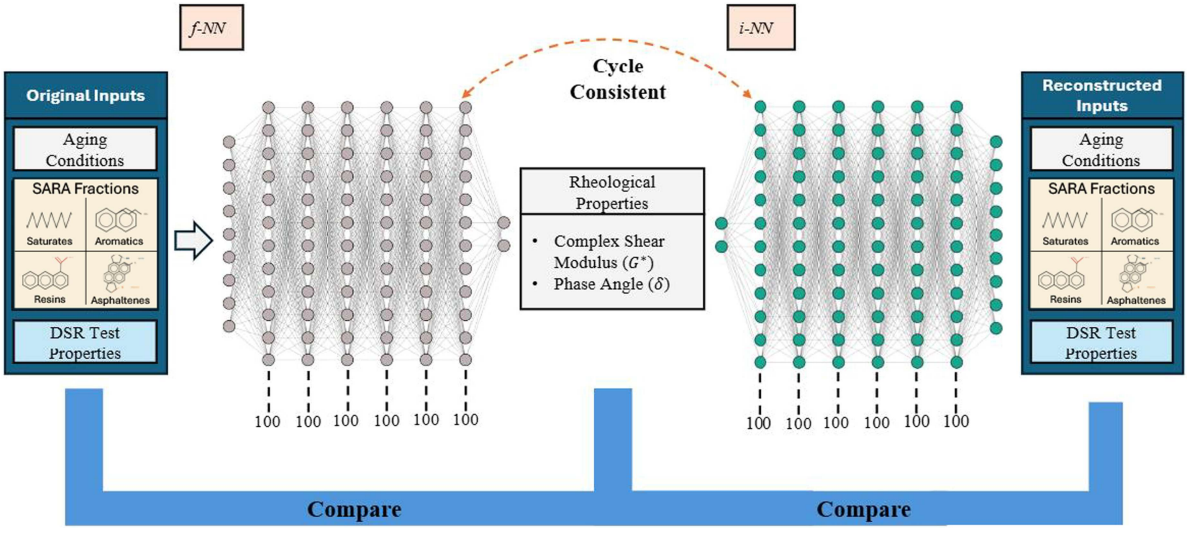


Figure 3. BidiNN architecture with cycle-consistency.

Each ensemble member $\mathcal{M}_k$ maintains the same architectural structure as the base model, including the encoder, forward mapping network and inverse mapping network. The perturbed models are set to evaluation mode without additional training, ensuring that the perturbations represent variations around the converged solution rather than random initialisations.

For inverse prediction, each ensemble member independently processes the same rheological input data y through its perturbed inverse network g_k:

$$\mathrm{x}_k = \mathrm{g}_k(\mathrm{y}), \quad k = 1, 2, \ldots, K, \tag{14}$$

generating a set of diverse solutions $\{\mathrm{x}_1, \mathrm{x}_2, \ldots, \mathrm{x}_K\}$ that represent different feasible compositions and processing conditions.

All ensemble-generated solutions undergo the same physical constraint validation as the base model to ensure practical feasibility. The constraint enforcement process ensures that SARA fractions sum to approximately 100%, maintains non-negative values for physical parameters such as time, pressure and frequency, enforces reasonable temperature ranges between −50 °C and 200 °C and bounds SARA component fractions within the interval [0, 100]. For SARA fraction normalisation, if the sum of predicted fractions exceeds 100%, a scaling factor is applied:

$$x_{k,i}^{\mathrm{SARA}} = x_{k,i}^{\mathrm{SARA}} \cdot \frac{100}{\sum_{j \in \mathrm{SARA}} x_{k,j}^{\mathrm{SARA}}}, \tag{15}$$

where $x_{k,i}^{\mathrm{SARA}}$ represents the i-th SARA component predicted by the k-th ensemble member. The ensemble size K is typically chosen between 5 and 10 members to balance solution diversity with computational efficiency. This range provides sufficient variation to capture the uncertainty in the inverse mapping while maintaining reasonable computational requirements. Each ensemble prediction is validated by forward-passing through the original base model to verify that the predicted compositions and conditions produce rheological properties consistent with the target values, ensuring that all generated solutions are both physically meaningful and mathematically consistent with the training data.

The ensemble methodology acknowledges the inherent non-uniqueness of the inverse problem by providing multiple valid pathways to achieve the same rheological performance, offering valuable insights into parameter sensitivity and process flexibility. This approach extends the deterministic framework to a probabilistic one, where the ensemble spread naturally quantifies the uncertainty associated with the inverse prediction task.

4 Results and discussion

4.1 Forward prediction performance

The BidiNN was evaluated for its accuracy in forward prediction in training and test sets, using the original input features to predict output variables G^* and δ. The results are depicted in Figure 4, which show scatter plots of the true versus predicted values for G^* and δ, with R^2 scores indicating the predictive performance of the model.

For the training set, the forward predictions achieved R^2 scores of 0.967 for G^* and 0.974 for δ, demonstrating a strong fit to the training data. The scatter plots reveal a tight alignment of predicted values along the diagonal, indicating that the model effectively captures the underlying relationships between the input features and the output variables. In the test set, the R^2 scores were slightly lower, 0.965 for G^* and 0.977 for δ, suggesting that the model generalises well to unseen data with minimal overfitting.

To assess the cycle-consistency of the BidiNN, the ability of the model to reconstruct the output variables (G^* and δ) was evaluated using reconstructed inputs derived from the inverse mapping ($Y \rightarrow X \rightarrow Y$). This process begins by mapping the true outputs (Y) to reconstructed inputs (X) through the inverse network, followed by predicting the outputs again via the forward network using these reconstructed inputs. The results are presented in Figure 5.

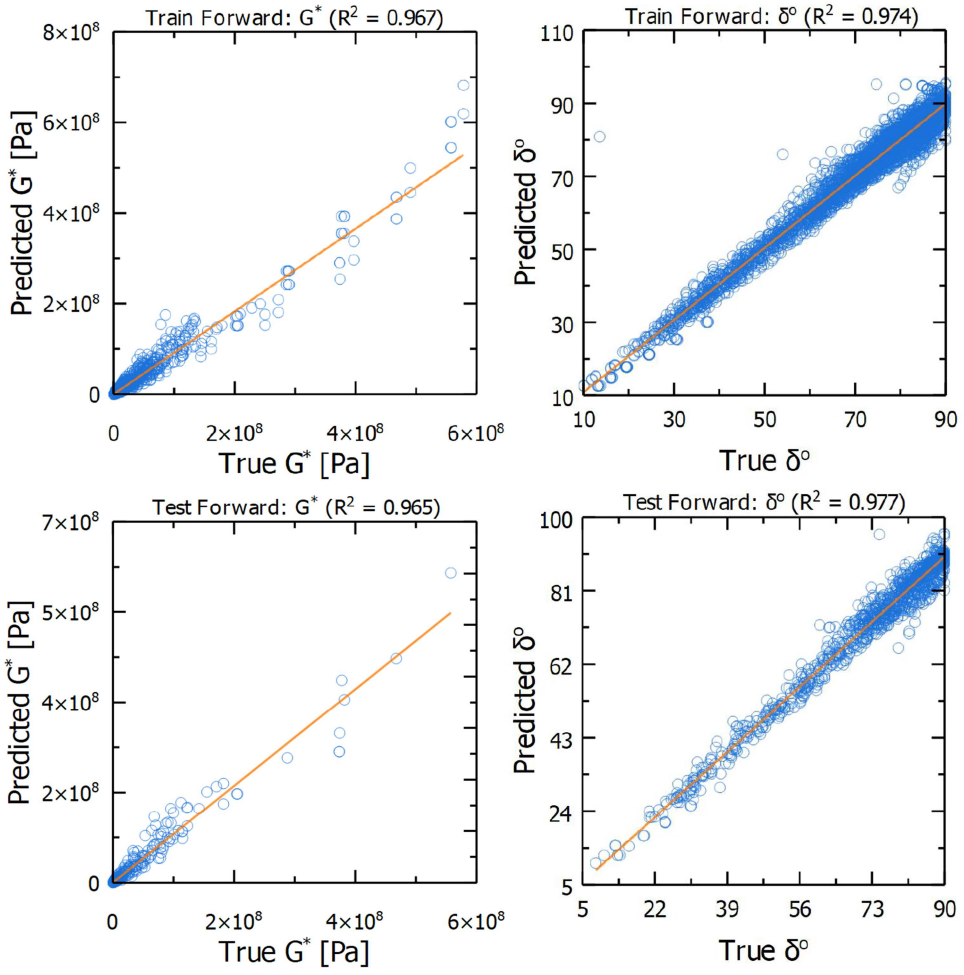


Figure 4. Training and testing performance of the BidiNN models in predicting G^* and δ of asphalt binder from the original inputs ($x \rightarrow y$). The scatter plots compare predicted and true values for G^* and δ for both training and testing datasets.

For the training and testing sets, the Y → X → Y cycle-consistency predictions yielded R^2 scores higher than 0.970 for G^* and 0.990 for δ. These high R^2 scores indicate robust cycle-consistency for both the G^* and the δ, with the model successfully reconstructing inputs that lead to accurate output predictions. The scatter plot for G^* shows a tight alignment along the diagonal, suggesting that the reconstructed inputs effectively preserve the information required to predict G^*.

4.2 Inverse design performance

The evaluation of BidiNN's inverse design performance reveals the inherently ill-posed nature of this problem. When attempting to reconstruct the input parameters from the output variables through the inverse mapping ($Y \rightarrow X$), significant limitations inherent to this type of problem become apparent.

As shown in Figures 6 and 7, the R^2 values for the reconstructed parameters range between 0.544 and 0.899, indicating varying levels of success in reconstruction. This substantial variation in R^2 values highlights the ill-posed nature of the inverse problem, where multiple combinations of input parameters can produce similar outputs, making exact reconstruction challenging.

Aromatics demonstrate the best reconstruction performance ($R^2 \approx 0.786$–0.790), suggesting a more direct relationship with the rheological properties of the asphalt binder. In contrast, Saturates show the weakest performance ($R^2 \approx 0.544$–0.536), indicating that their influence on the output properties may be more complex or more intertwined with other parameters.

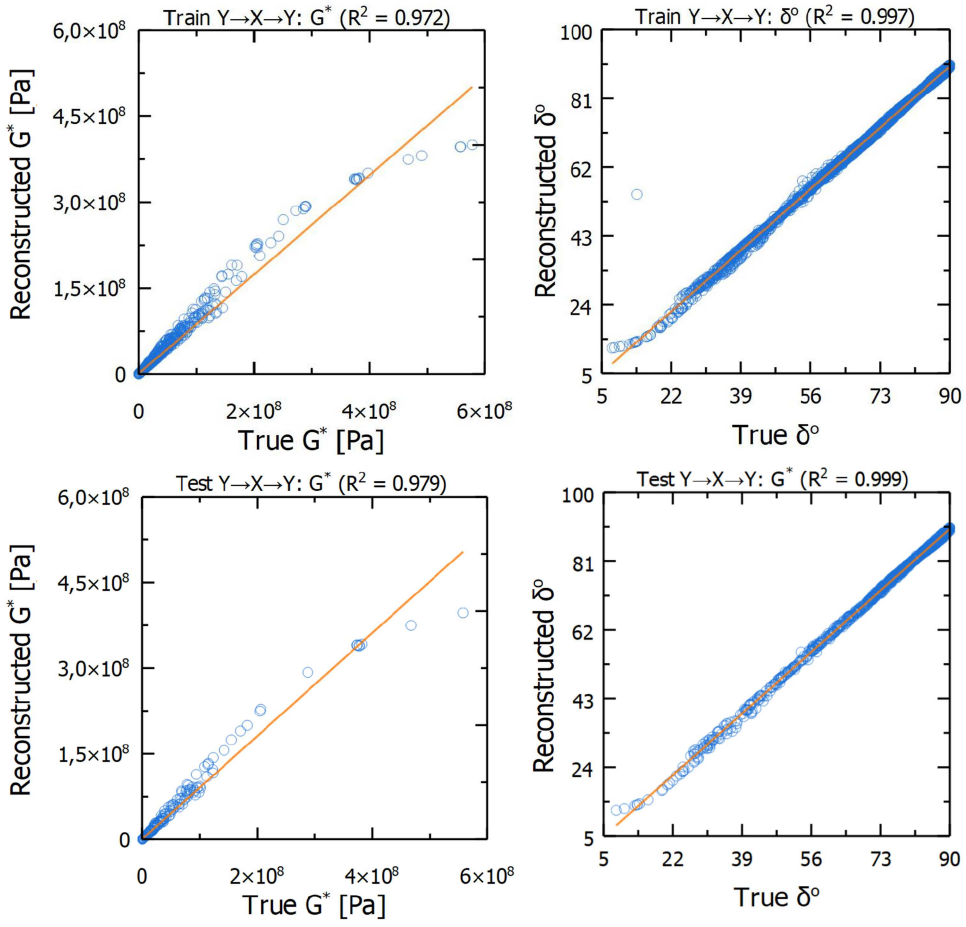


Figure 5. Training and testing performance of the BidiNN models in predicting G^* and δ of asphalt binder from the reconstructed inputs ($y \rightarrow x \rightarrow y$). The scatter plots compare reconstructed and true values for G^* and δ for both training and testing datasets.

However, despite the variations in reconstructing individual parameters, the model maintains high accuracy in predicting G^* when using these reconstructed parameters. This remarkable result confirms that the BidiNN has successfully captured the essential physics of the system, identifying alternative but equally valid parameter combinations that preserve the critical rheological behaviour. This capability is valuable for materials design, where discovering multiple pathways to achieve desired properties offers greater flexibility in manufacturing and formulation.

4.3 Rheological analysis and inverse design of asphalt binders using BidiNN: SARA composition and viscoelastic behaviour

The BidiNN model undergoes a comprehensive evaluation to assess the performance in predicting the rheological behaviour of asphalt binders from their SARA compositions. Three representative asphalt binder formulations—S-A52-62, H-C92-28A and F-A53-60—are analysed, each reflecting a different chemical design space, marked by distinct SARA distributions and varying degrees of colloidal stability.

Table 5 defines seven key indices derived from the SARA fractions. The Colloidal Instability Index (CII) represents the ratio of Saturates and Asphaltenes to Aromatics and Resins, with higher values indicating greater colloidal instability. The Saturates to Aromatics ratio (S/A) reflects the binder's solvency power. The Aromaticity Index measures the dominance of aromatic components. The Polar Compound Ratio (PCR) evaluates the proportion of polar to non-polar fractions. The Resin to Asphaltene Ratio (R/As) and Aromatics to Asphaltene Ratio (A/As) assess the stabilisation and solvency of Asphaltenes, respectively.

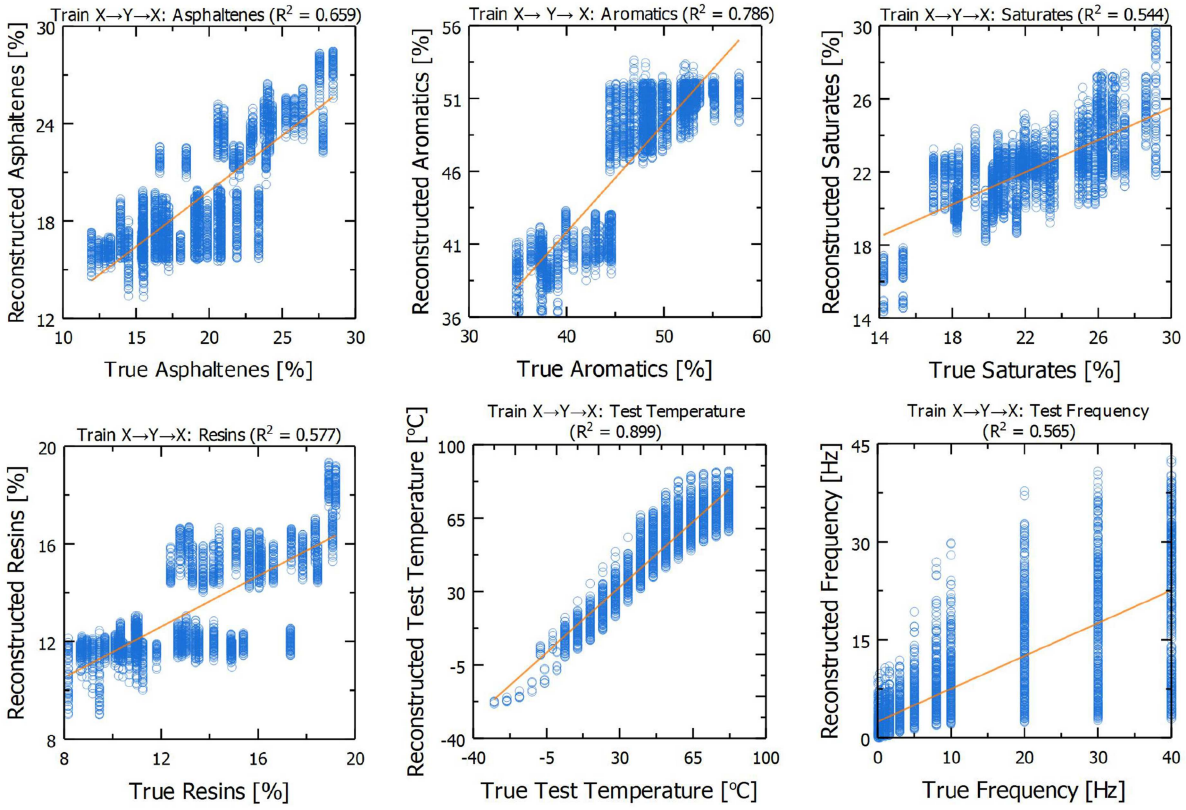


Figure 6. Training performance of the BidiNN models in predicting the design parameters of asphalt binder. The scatter plots compare reconstructed and true values for the asphaltenes, aromatics, saturates, test temperature and test frequency.

Lastly, the Peptisation Parameter indicates the ability of Resins and Aromatics to disperse Asphaltenes, with higher values linked to better dispersion. Table 6 applies these indices to the three binders, revealing distinct compositional profiles.

4.3.1 Standard binder S-A52-62 – forward prediction

The first composition selected for analysis, Binder S-A52-62, is characterised by a high asphaltene ratio, with CII of 0.62 (Figure 8). The SARA fractions are as follows: Saturates at 21.0%, Aromatics at 53.0%, Resins at 9.0% and Asphaltenes at 17.0%. Predictions from the BidiNN were generated across a frequency range of 0 to 10 Hz and a temperature range of 20 °C to 80 °C, allowing for a comprehensive assessment of the viscoelastic properties under varying conditions.

G^*, as predicted by the BidiNN, exhibits a logarithmic increase with decreasing frequency, a behaviour consistent with viscoelastic relaxation. At 20 °C, G^* ranges from approximately 7.0 E5 Pa at 0 Hz to 1.0 E7 Pa at 10 Hz, while at 80 °C, it drops significantly over the same frequency span. δ decreases with both frequency and temperature. At 20 °C δ varies from approximately 73 °C to 55 °C, whereas at 80 °C, δ drops from 89° to 87°. This shift indicates a transition from predominantly elastic to more viscous behaviour. The sensitivity analysis underscores the BidiNN's ability to capture these intricate dependencies, validating its predictive power. The high asphaltene fraction likely drives the observed temperature sensitivity, providing critical insights into the rheological behaviour of such materials under the tested conditions.

4.3.2 Binder H-C92-28A (high CII) – forward prediction

The ability of the BidiNN to predict rheological properties for an asphalt binder characterised by a high CII is evaluated (Figure 9). The binder's SARA fractions consist of Saturates (28.0%), Aromatics (41.0%), Resins (11.0%) and Asphaltenes (20.0%), resulting in a CII of 0.92, indicating a borderline unstable

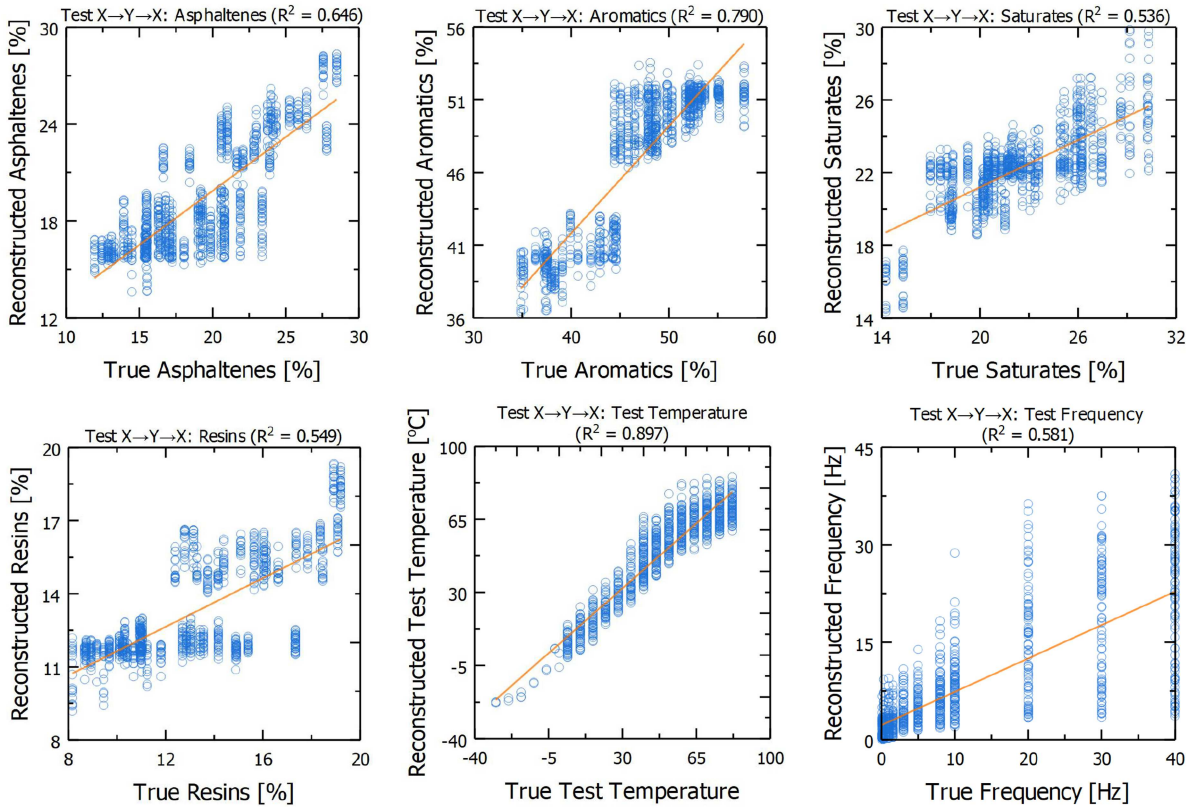


Figure 7. Testing performance of the BidiNN models in predicting the design parameters of asphalt binder. The scatter plots compare reconstructed and true values for the asphaltenes, aromatics, saturates, test temperature and test frequency.

Table 5. SARA-derived indices formulas.

Parameter	Formula
Colloidal instability index (CII)	$\frac{S + As}{A + R}$
Saturates to aromatics (S/A)	$\frac{S}{A}$
Aromaticity index	$\frac{A}{S + R}$
Polar compound ratio (PCR)	$\frac{R + As}{S + A}$
Resin to asphaltene ratio (R/As)	$\frac{R}{As}$
Aromatics to asphaltene ratio (A/As)	$\frac{A}{As}$
Peptisation parameter	$\frac{R + A}{As}$

Table 6. SARA-derived indices values and interpretations.

Parameter	S-A52-62	H-C92-28A	F-A53-60
(CII)	0.62 (Stable system)	0.92 (Borderline unstable)	0.60 (Stable system)
(S/A)	0.41 (Good solvency)	0.68 (Lower solvency power)	0.34 (Good aromatic solvency)
Aromaticity index	1.84 (Strong aromatic character)	1.05 (Balanced aromatic character)	1.89 (Strong aromatic character)
(PCR)	0.40 (Moderate polarity)	0.45 (Moderate polarity)	0.42 (Moderate polarity)
(R/As)	0.53 (Borderline stabilisation)	0.55 (Marginal stabilisation)	0.50 (Borderline stabilisation)
(A/As)	3.08 (Good solvency)	2.05 (Moderate solvency)	2.65 (Good solvency)
Peptisation parameter	3.61 (Strong dispersion)	2.60 (Fair dispersion potential)	3.15 (Strong dispersion potential)

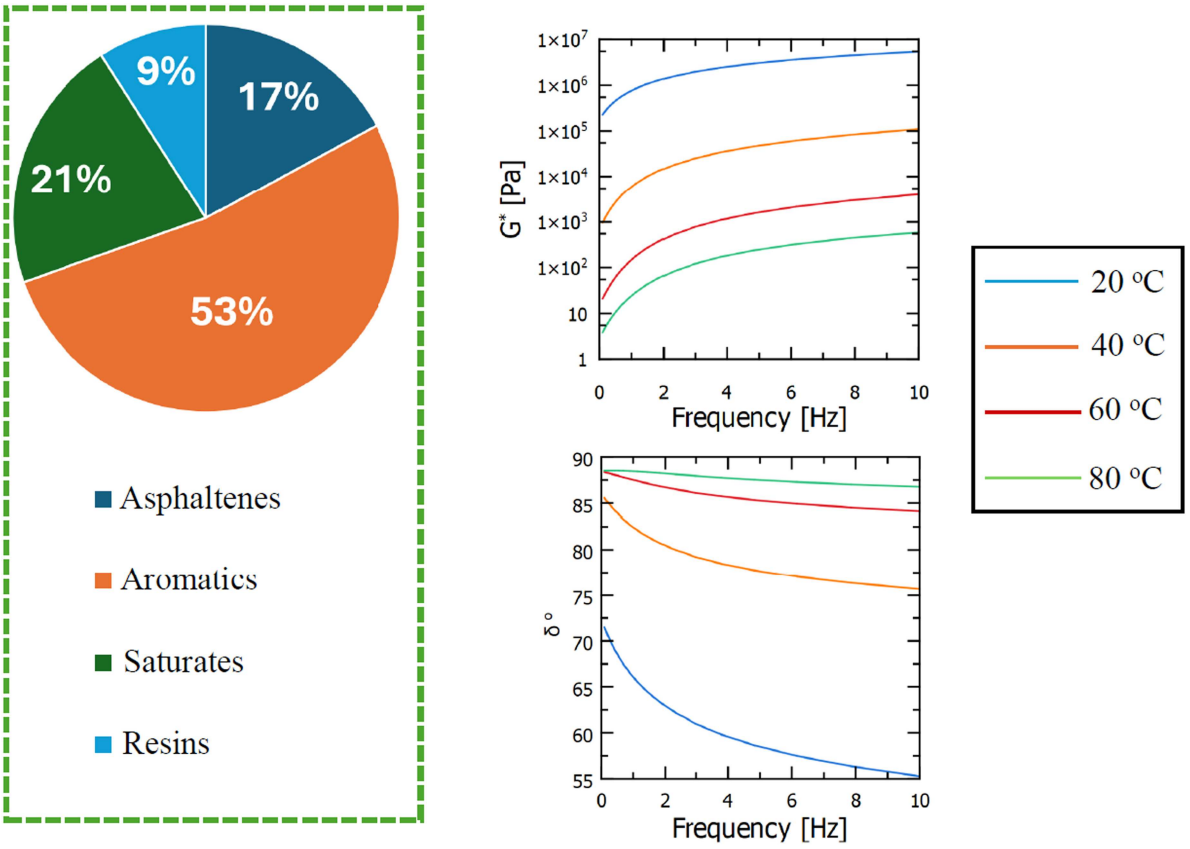


Figure 8. SARA composition and rheological behaviour of binder S-A52-62. The ternary diagram (left) illustrates the SARA fractions (Saturates: 21.0%, Aromatics: 53.0%, Resins: 9%, Asphaltenes: 17.0%) with CII of 0.62. The plots (right) show G^* and δ as functions of frequency (0–10 Hz) at temperatures of 20 °C, 40 °C, 60 °C and 80 °C, highlighting the influence of temperature and frequency on viscoelastic properties.

colloidal system. A high CII suggests reduced asphaltene dispersion, potentially leading to increased stiffness and susceptibility to cracking.

The BidiNN generated forward predictions for G^* and δ across a frequency range of 0 Hz to 10 Hz and temperatures of 20 °C, 40 °C, 60 °C and 80 °C (Figure 9). The plots on the right show predicted G^* and δ as functions of frequency at the specified temperatures. The predicted trends are consistent with established rheological behaviour of asphalt binders: G^* decreases with increasing temperature due to reduced viscosity, while δ increases, indicating a shift toward more viscous behaviour at higher temperatures.

The analysis demonstrates the BidiNN's capability to predict rheological outcomes for binders with high CII, providing valuable insights for designing asphalt mixtures that balance stiffness and flexibility under varying environmental conditions. The model's success in this challenging scenario validates its potential for practical applications in pavement engineering, particularly for formulations prone to colloidal instability.

4.3.3 Binder F-A53-60 (high aromatics) – forward prediction

The predictive capability of the BidiNN model for the rheological properties of an asphalt binder with a high aromatic content is also evaluated. Figure 10 displays the predicted rheological responses across frequencies at each temperature. As expected, G^* decreases with rising temperature due to reduced viscosity, while δ increases, indicating a transition toward more viscous behaviour. At 20 °C, the binder's high aromatic fraction (53.0%) results in a lower G^* compared to the high-CII binder, reflecting its softer, more flexible nature. With increasing frequency, G^* rises—especially at lower temperatures while δ declines, suggesting a more elastic response, modulated by the influence of the aromatic-rich composition.

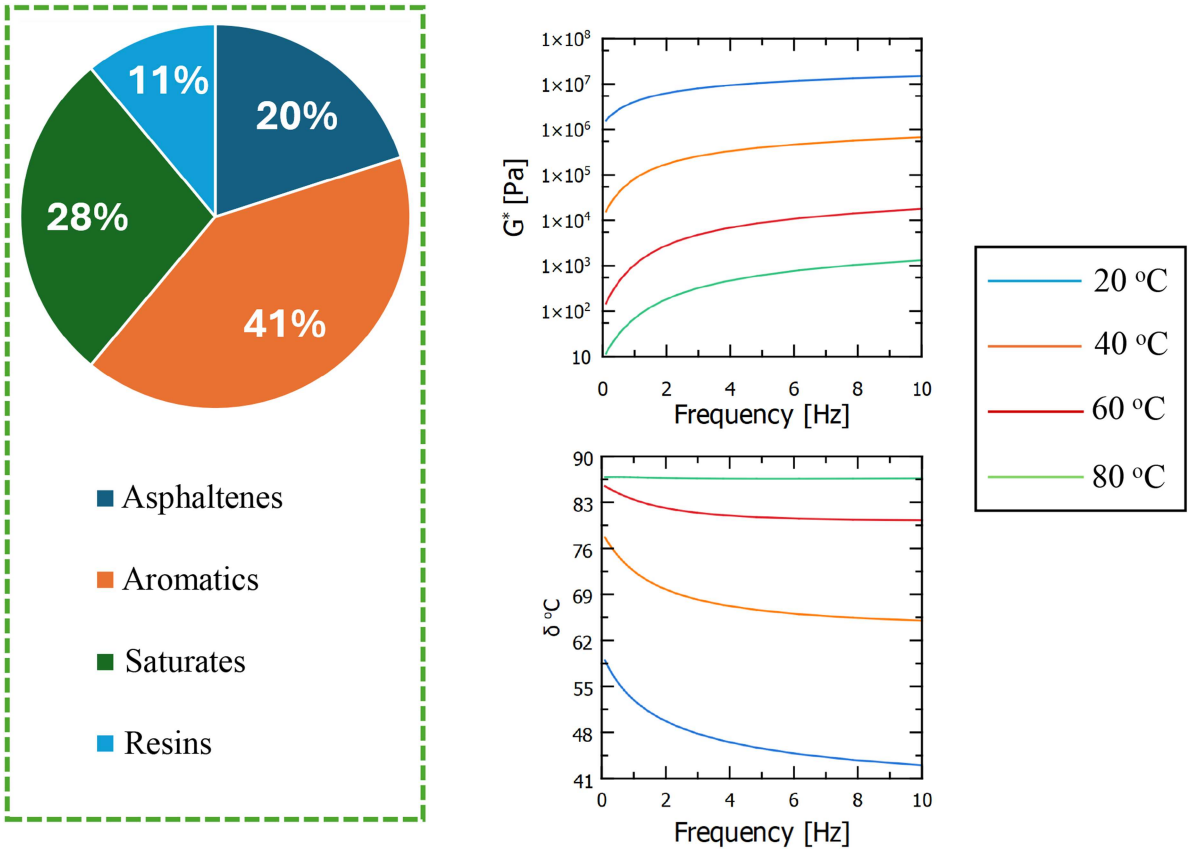


Figure 9. SARA composition and rheological behaviour of binder H-C92-28A. The ternary diagram (left) illustrates the SARA fractions (Saturates: 28.0%, Aromatics: 41.0%, Resins: 11.0%, Asphaltenes: 20.0%) with a colloidal index (CII) of 0.92. The plots (right) show G^* and δ as functions of frequency (0–10 Hz) at temperatures of 20 °C, 40 °C, 60 °C and 80 °C, highlighting the influence of temperature and frequency on viscoelastic properties.

The analysis demonstrates the BidiNN's capability to predict rheological outcomes for binders with high aromatic content, providing valuable insights for designing asphalt mixtures that prioritise flexibility and fatigue resistance under varying environmental conditions.

4.3.4 Binders S-A52-62, H-C92-28A, F-A53-60 – inverse prediction

The evaluation of BidiNN's inverse design capabilities involves examining its ability to reconstruct SARA compositions from rheological properties for the three previously characterised binders. Figure 11 presents the predicted SARA distributions obtained through inverse mapping (G^* and $\delta \rightarrow$ SARA fractions).

For binder S-A52-62, the BidiNN model reconstructs a SARA distribution that preserves the original proportional relationships. The inverse model estimates a slightly lower Aromatics content (around 51% compared to the original 53%) and a slightly higher Resins content (11% predicted versus 9% original). The proportions of Asphaltenes and Saturates remain unchanged. Despite these minor differences, the predicted composition exhibits similar colloidal stability, as indicated by a comparable colloidal index (CI) of 0.60 versus 0.62, supporting the expectation of similar rheological behaviour.

The reconstruction of binder H-C92-28A, characterised by a high CII composition, most clearly illustrates the ill-posed nature of the inverse problem. The predicted SARA distribution reveals a more pronounced shift, with Asphaltenes content increasing to approximately 23% (compared to the original 20%) and Saturates decreasing to about 21% (from the original 28%). Despite this redistribution, the model preserves the binder's core rheological characteristics by maintaining a relatively high Aromatics content.

For binder F-A53-60, the reconstructed composition again presents an alternative formulation with slightly lower aromatic content (approximately 47% versus the original 53%) and subtle adjustments in other fractions. The model identifies an alternative SARA distribution that would yield nearly identical

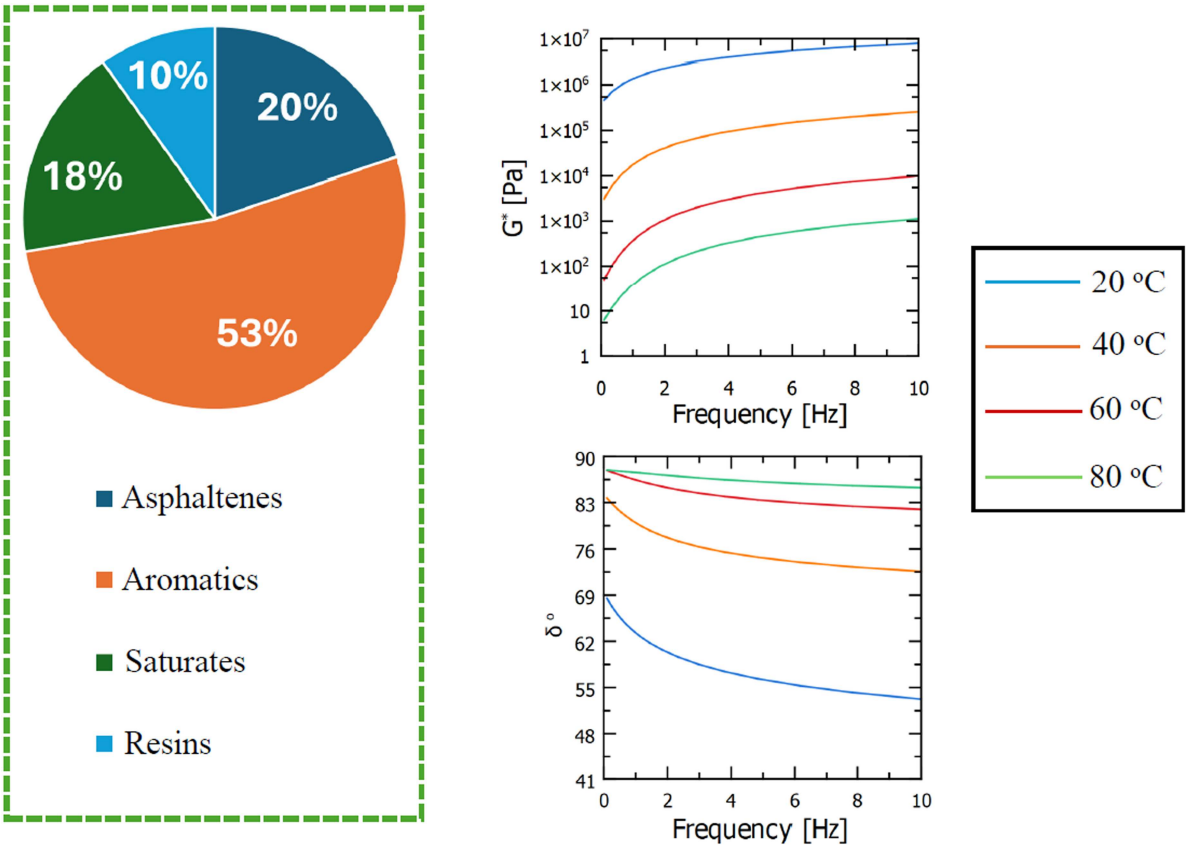


Figure 10. SARA composition and rheological behaviour of binder F-A53-60. The ternary diagram (left) illustrates the SARA fractions (Saturates: 18.0%, Aromatics: 53.0%, Resins: 10.0%, Asphaltenes: 20.0%) with a colloidal index (CII) of 0.60. The plots (right) show G^* and δ as functions of frequency (0–10 Hz) at temperatures of 20 °C, 40 °C, 60 °C and 80 °C, highlighting the influence of temperature and frequency on viscoelastic properties.

viscoelastic properties while maintaining the essential character of a stable system dominated by aromatic components.

These findings demonstrate a critical insight into the inverse design problem: multiple SARA compositions can yield virtually identical rheological properties. This apparent limitation actually represents a valuable feature for materials design, as it reveals the solution space of viable formulations that satisfy target performance criteria. When these reconstructed compositions are fed back through the forward model, they produce G^* and δ values remarkably close to those of the original binders ($R^2 > 0.97$), confirming that the BidiNN has successfully captured the underlying physics governing asphalt binder behaviour.

The variations between original and reconstructed compositions can be attributed to the inherent many to one mapping between chemical composition and rheological properties, where different molecular arrangements can produce similar mechanical responses. Complex interactions between SARA fractions create balancing effects, allowing shifts in one component to be balanced by adjustments in others. The presence of certain rheological invariants, such as CII, when preserved, maintain similar viscoelastic characteristics despite compositional differences.

4.4 Validation of multiple solutions

Figure 12 reveals a diverse yet consistent set of SARA compositions. The SARA Composition vs Frequency plot shows that Aromatics dominate across frequencies, stabilising near 45% at higher frequencies (40 Hz), while Saturates, Asphaltenes and Resins exhibit flatter trends, ranging between 14–34%. The Average SARA Composition pie chart indicates an overall distribution of 44% Aromatics, 22% Saturates, 21%

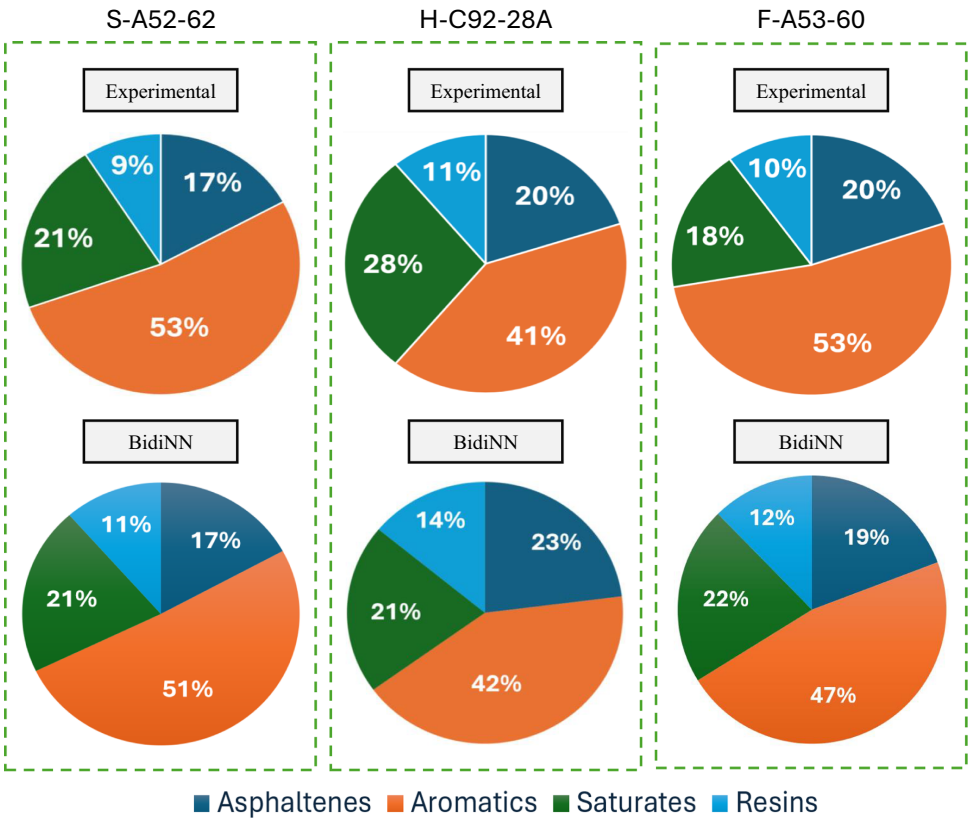


Figure 11. Predicted SARA fraction distributions for asphalt binders S-A52-62, H-C92-28A and F-A53-60 using BidiNN.

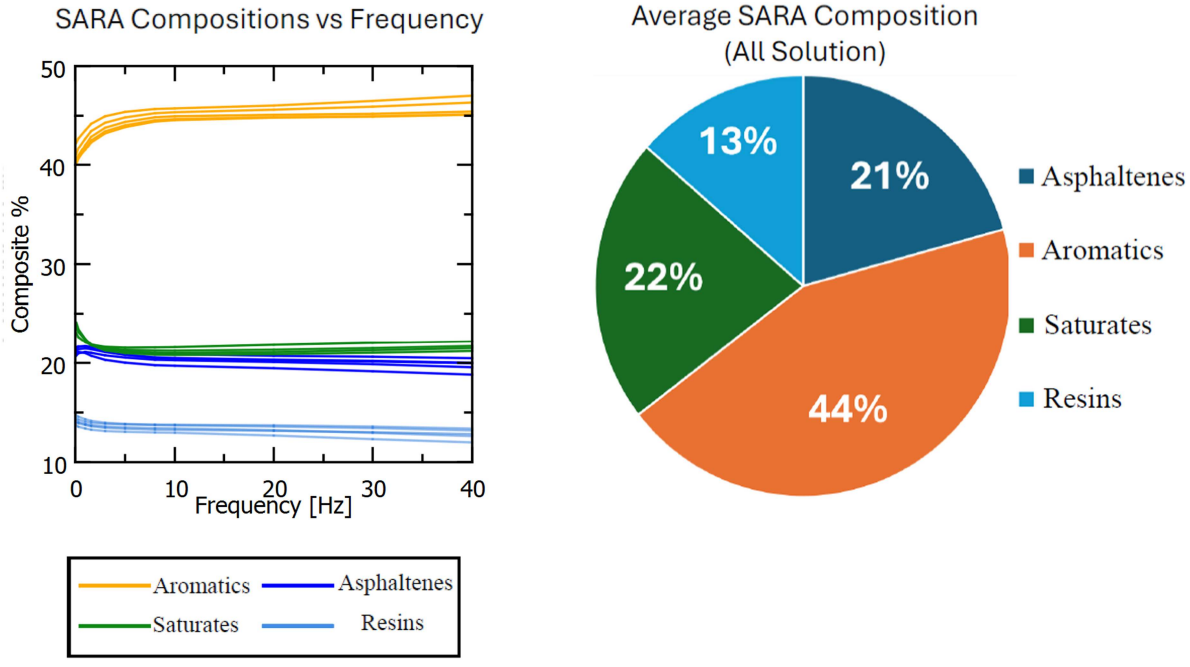


Figure 12. Prediction results of the LTA binder – SARA composition trends across frequencies and average distribution (all solutions).

Asphaltenes and 13% Resins, highlighting Aromatics as the primary component. The Solution Diversity bar chart further demonstrates variability, with Aromatics showing the highest standard deviation (1.76%), suggesting greater uncertainty in their prediction compared to Saturates (0.89%), Asphaltenes (0.67%) and Resins (0.53%) (Figure 13). This variability highlights the ability of the model to capture a range of plausible solutions, reflecting the inherent complexity and non-uniqueness of inverse predictions for SARA fractions from rheological data based on the trained BidiNN.

5 Discussion: comparative analysis of SARA compositions and implications for rejuvenator design

The BidiNN model exhibits robust predictive performance with no signs of overfitting, as evidenced by the close convergence of training and testing losses across all loss components (Figure 14). This reliability enables confident interpretation of the model's insights into the relationship between SARA fractions and

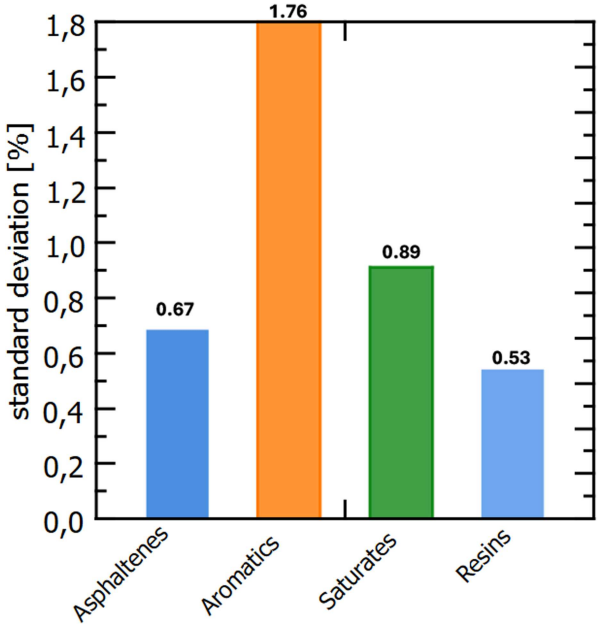


Figure 13. Prediction variability of the LTA binder – standard deviation of SARA components across predicted solutions.

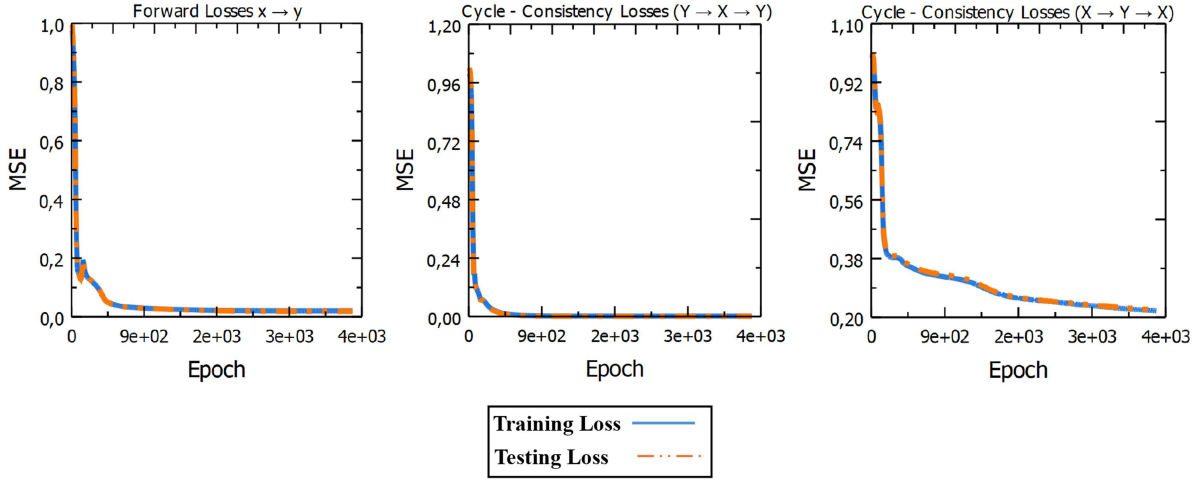


Figure 14. Training and testing loss curves for the BidiNN model across forward and cycle-consistency mappings.

rheological behaviour. The analysis of three distinct binder compositions reveals how SARA fractionation influences viscoelastic response under varied temperature and loading conditions, offering valuable guidance for rejuvenator design and application strategies.

The standard binder S-A52-62, characterised by a moderate (CII) of 0.62 and a high aromatic content (53.0%), exhibits well-balanced viscoelastic properties. The high peptisation parameter (3.61) suggests effective asphaltene dispersion within the maltene phase, contributing to this balanced rheological profile. This composition serves as an effective baseline for evaluating the other binders and potential rejuvenation strategies. Interestingly, the BidiNN model also succeeded in recovering the composite structure of S-A52-62. The predicted composition (17.0% Asphaltenes, 51.0% Aromatics, 21% Saturates and 11% Resins) aligns remarkably well with the experimental values of 17.0%, 53.0%, 21.0% and 9.0%, respectively. This close match highlights the ability of the model to capture the balance of components that define the binder's viscoelastic behaviour. The slight overestimation of Resins and underestimation of Aromatics may reflect the sensitivity of the model to the peptisation dynamics, yet the overall fidelity suggests that S-A52-62 represents a stable and reproducible formulation. This makes it not only a reliable benchmark for evaluating alternative binders but also a valuable reference point for guiding rejuvenation strategies through inverse design.

In contrast, binder H-C92-28A with its elevated CII (0.92) approaches the threshold of colloidal instability due to the higher saturate (28.0%) and asphaltene (20.0%) contents relative to its aromatic (41.0%) and resin (11.0%) fractions. The reduced peptisation parameter (2.60) indicates less effective asphaltene dispersion, contributing to different rheological characteristics. In addition, the BidiNN model does not perfectly replicate the experimental composition of H-C92-28A (predicting 23% Asphaltenes, 14% Resins, 42% Aromatics and 21% Saturates). However, the alternative composite predicted similar G^* and δ. This suggests that while the compositional match is approximate, the model effectively internalises the functional relationships between component fractions and viscoelastic response. Such predictive robustness is especially valuable for binders near the colloidal instability threshold, where small compositional shifts can lead to significant performance changes.

The high-aromatic binder F-A53-60, with its substantial aromatic fraction (53.0%) and moderate CII (0.60), demonstrates enhanced flexibility characteristics. The BidiNN predictions show that this composition exhibits lower G^* values compared to H-C92-28A, particularly at lower temperatures, reflecting the softening effect of the elevated aromatic content. The peptisation parameter of 3.15 indicates good asphaltene dispersion, though not as optimal as S-A52-62, aligning with its observed rheological behaviour. For this binder, the reconstructed inputs were also compared with the original composite. The results show that the inverse predictions for F-A53-60 closely approximate the true input values, particularly in terms of aromatic content and CII, indicating the model's robustness in capturing the underlying structure-property relationships.

For aged binders resembling the high-CII composition (H-C92-28A), rejuvenators should prioritise aromatic replenishment to reduce the CII toward more stable values (0.6–0.7), improving asphaltene dispersion and decreasing brittleness. The BidiNN model suggests that increasing the aromatic fraction from 41% to approximately 52% (similar to S-A52-62 or F-A53-60) would significantly improve the rheological profile, particularly at lower temperatures where brittleness is most problematic. Conversely, for binders that have been over-rejuvenated toward excessive aromatic content (approaching F-A53-60's composition), the model indicates that slight increases in asphaltene or saturate contents could provide beneficial stiffening effects without compromising flexibility. This nuanced approach to rejuvenator formulation represents a significant advancement over traditional methods that focus solely on softening the aged binder without consideration for optimal SARA balance.

6 Limitations and future directions

The dataset, comprising 5830 data points from 70 asphalt binders, provides a robust foundation but remains limited to specific binder types and aging conditions, namely fresh and PAV-aged states. The dataset excludes polymer-modified binders and non-standard aging protocols such as UV exposure, which limits generalisation to real-world pavement scenarios. Extending the framework to modified binders would require additional

input features describing modifier type and concentration. Aging conditions were encoded as three continuous physical variables—aging temperature, time and pressure—which is more informative than a simple categorical label, but still fails to fully represent the continuous and dynamic nature of oxidative aging under field conditions, limiting predictions for non-standard environmental exposures such as UV radiation or thermo-oxidative cycling. The ensemble approach, while addressing non-uniqueness, increases computational demands, posing challenges for real-time or large-scale applications.

Finally, the proposed rejuvenation strategies, such as increasing aromatic content to reduce CII, lack experimental validation, as predictions remain untested in laboratory settings. A further limitation concerns the method-dependence of SARA fractionation. Different analytical procedures, including SPE, gravimetric adsorption chromatography, TLC-FID and HPLC employ different solvents, stationary phases and elution sequences, which can yield systematically different fraction weights for the same binder material. In the present study, all fractionation was performed using a single standardised SPE protocol (Section 2.1), ensuring internal consistency across the dataset. As a consequence, the trained BidiNN is strictly applicable to SARA data obtained by this specific procedure. Direct use of fractions produced by alternative methods would introduce systematic input errors and would likely degrade model performance. Transferability across laboratories and analytical methods therefore requires either method harmonisation or re-training on method-matched datasets, which represents an important constraint on the broader applicability of the framework. Related to this, the model relies solely on the bulk weight percentages of the four SARA fractions, without accounting for the molecular heterogeneity within each fraction.

Literature has clearly demonstrated that binders with identical SARA weight distributions can exhibit substantially different rheological behaviour depending on the detailed molecular composition of their constituents—including the degree of aromaticity, alkyl side-chain length and branching, heteroatom content and molecular weight distribution within each fraction. This many-to-one relationship between bulk SARA composition and molecular structure represents a fundamental limitation of SARA-based modelling approaches in general, and the BidiNN framework is no exception. The current model may therefore overlook subtle chemical effects that are critical for specific performance characteristics, particularly when comparing binders from different crude oil sources or refinery processes. Addressing these limitations points to several promising directions for future work. Incorporating more detailed chemical descriptors as additional input features—such as polarity indices, molecular weight distributions, or spectroscopic fingerprints from FTIR or NMR—could substantially improve the specificity and transferability of the inverse design framework.

Advanced techniques such as embedding physical or chemical constraints directly into the loss function could better constrain the inverse design space. Exploring Bayesian neural networks or generative adversarial networks may further quantify uncertainty and improve the precision of SARA composition predictions. Expanding the dataset to include diverse asphalt binders, such as those modified with polymers, bio-based additives, or recycled asphalt pavement materials, would enhance model robustness; the proposed bidirectional and cycle-consistent BidiNN framework is well suited for this extension, as it can accommodate higher-dimensional feature spaces while maintaining consistent forward and inverse mappings, which becomes increasingly important as the inverse problem grows more ill-posed with added material complexity. Incorporating varied aging conditions, including UV exposure or field-aged binders, would better reflect real-world scenarios. Finally, experimental validation of the proposed rejuvenation strategies—such as adjusting aromatic or resin fractions to optimise CII—requires laboratory testing with bio-based or petroleum-derived rejuvenators to confirm predicted improvements in viscoelastic properties. Pursuing these directions can transform the BidiNN framework into a more robust and versatile tool for asphalt binder design, advancing the development of sustainable and durable pavement solutions.

7 Conclusion

The bidirectional neural network framework developed in this study represents a promising computational approach to predicting and designing asphalt binders by effectively capturing the intricate relationship between chemical composition and rheological performance. SARA fractions serve as the foundation for the model, enabling precise forward predictions of viscoelastic properties, such as complex modulus and phase angle, while facilitating robust inverse design to determine optimal chemical compositions for desired performance outcomes. Cycle-consistency losses ensure dependable bidirectional mappings, addressing the non-uniqueness of the inverse problem through an ensemble approach that generates multiple feasible SARA compositions.

This methodology deepens the understanding of how chemical constituents influence binder behaviour under diverse environmental and loading conditions, providing a valuable computational basis for exploring asphalt formulations aimed at enhancing pavement durability and sustainability. Application to real-world datasets, including both aged and unaged binders, highlights the potential of this framework to advance asphalt binder design by offering data-driven insights into the complex interplay between SARA composition and viscoelastic response.

It is important to acknowledge, however, that the present work constitutes an exploratory and enabling step rather than a fully validated design tool for practical formulation. The proposed design implications, including SARA-based rejuvenation strategies and targeted compositional adjustments, are derived from computational predictions and remain to be confirmed through systematic experimental validation. Furthermore, the framework relies on bulk SARA weight fractions and does not account for the molecular heterogeneity within each fraction, which represents a fundamental limitation shared with SARA-based modelling approaches in general. Bridging this gap will require richer chemical characterisation and systematic laboratory validation of the predicted rejuvenation strategies.

Acknowledgements

The financial support by the Austrian Federal Ministry for Digital and Economic Affairs, the National Foundation for Research, Technology and Development and the Christian Doppler Research Association [grant number 1836999] is gratefully acknowledged by the authors. Furthermore, the authors would also like to express their gratitude to the CD Laboratories' company partners BMI Group, OMV Downstream and Pittel + Brausewetter for their financial support. In addition, this publication is part of the project 'A multiscale approach towards future road infrastructure: How to design sustainable paving materials?' (project number 18148) of the research program NWO Talent Programme Veni AES 2020, which is awarded to A.V. and financed by the Dutch Research Council (NWO).

Author contributions

CRediT: **Mahmoud Khadijeh:** Investigation, Methodology, Validation, Visualization, Writing – original draft, Writing – review & editing.

Disclosure statement

No potential conflict of interest was reported by the author(s).

ORCID

Mahmoud Khadijeh 0009-0006-5186-6754
Sophie Stüwe 0009-0000-9994-6661
Johannes Mirwald 0000-0001-5025-7427
Bernhard Hofko 0000-0002-8329-8687
Lukas Eberhardsteiner 0000-0003-2153-9315
Aikaterini Varveri 0000-0002-8830-9437

References

Ashoori, S., Sharifi, M., Masoumi, M., & Mohammad Salehi, M. (2017). The relationship between sara fractions and crude oil stability. *Egyptian Journal of Petroleum*, *26*(1), 209–213. https://doi.org/10.1016/j.ejpe.2016.04.002

Cavalli, M., Zaumanis, M., Mazza, E., Partl, M., & Poulikakos, L. (2018). Effect of ageing on the mechanical and chemical properties of binder from rap treated with bio-based rejuvenators. *Composites Part B: Engineering*, *141*, 174–181. https://doi.org/10.1016/j.compositesb.2017.12.060

Genzel, M., Macdonald, J., & März, M. (2022). Solving inverse problems with deep neural networks–robustness included? *IEEE Transactions on Pattern Analysis and Machine Intelligence*, *45*(1), 1119–1134. https://doi.org/10.1109/TPAMI.2022.3148324

Jiang, J., Guo, X., Hao, P., Guo, X., Huang, S., & Chen, K. (2024). Effects of sara fractions on the rheological properties and microscopic behavior of hard asphalt. *Construction and Building Materials*, *438*, 137055. https://doi.org/10.1016/j.conbuildmat.2024.137055

Kakar, M. R., Refaa, Z., Worlitschek, J., Stamatiou, A., Partl, M. N., & Bueno, M. (2019). Effects of aging on asphalt binders modified with microencapsulated phase change material. *Composites Part B: Engineering*, *173*, 107007. https://doi.org/10.1016/j.compositesb.2019.107007

Karevan, A., Zirrahi, M., & Hassanzadeh, H. (2022). Standardized high-performance liquid chromatography to replace conventional methods for determination of saturate, aromatic, resin, and asphaltene (sara) fractions. *ACS Omega*, *7*(22), 18897–18903. https://doi.org/10.1021/acsomega.2c01880

Khadijeh, M., Kasbergen, C., Erkens, S., & Varveri, A. (2025). Exploring the roles of numerical simulations and machine learning in multiscale paving materials analysis: Applications, challenges, best practices. *Computer Methods in Applied Mechanics and Engineering*, *433*, 117462. https://doi.org/10.1016/j.cma.2024.117462

Kheirollahi, S., BinDahbag, M., Bagherzadeh, H., Abbasi, Z., & Hassanzadeh, H. (2024). Improved determination of saturate, aromatic, resin, and asphaltene (sara) fractions using automated high-performance liquid chromatography approach. *Fuel*, *371*, 131884. https://doi.org/10.1016/j.fuel.2024.131884

Kumar, S., Tan, S., Zheng, L., & Kochmann, D. M. (2020). Inverse-designed spinodoid metamaterials. *npj Computational Materials*, *6*(1), 73. https://doi.org/10.1038/s41524-020-0341-6

Li, Z., Cao, X., Li, J., & Yang, X. (2025). Research on the correlation between the chemical components and the macroscopic properties of asphalt binder. *Materials*, *18*(3), 610. https://doi.org/10.3390/ma18030610

Liu, S., & Shan, L. (2025). Unraveling the molecular-micellar-colloidal structure of asphalt: From interactions to structural formation. *Composites Part B: Engineering*, *305*, 112718. https://doi.org/10.1016/j.compositesb.2025.112718

Ma, X., Ma, X., Wang, Z., Song, S., & Sheng, Y. (2023). Investigation of changing sara and fatigue properties of asphalt bitumen under ageing and analysis of their relation based upon the bp neural network. *Construction and Building Materials*, *394*, 132163. https://doi.org/10.1016/j.conbuildmat.2023.132163

Mansourkhaki, A., Ameri, M., Habibpour, M., & Shane Underwood, B. (2020). Chemical composition and rheological characteristics of binders containing RAP and rejuvenator. *Journal of Materials in Civil Engineering*, *32*(4), 04020026. https://doi.org/10.1061/(ASCE)MT.1943-5533.0003016

Mikhailenko, P., & Baaj, H. (2019). Comparison of chemical and microstructural properties of virgin and reclaimed asphalt pavement binders and their saturate, aromatic, resin, and asphaltene fractions. *Energy & Fuels*, *33*(4), 2633–2640. https://doi.org/10.1021/acs.energyfuels.8b03414

Mior Sani, W. N. H., Jaya, R. P., Masri, K. A., Saptaji, K., & Dulaimi, A. (2024). Exploring the chemical properties and microstructural characterisations of hybrid asphalt binders for enhanced performance. *Discover Applied Sciences*, *6*(4), 193. https://doi.org/10.1007/s42452-024-05868-4

Mirwald, J., Nura, D., & Hofko, B. (2022). Recommendations for handling bitumen prior to FTIR spectroscopy. *Materials and Structures*, *55*(2), 26. https://doi.org/10.1617/s11527-022-01884-1

Mirwald, J., Werkovits, S., Camargo, I., Maschauer, D., Hofko, B., & Grothe, H. (2020). Understanding bitumen ageing by investigation of its polarity fractions. *Construction and Building Materials*, *250*, 118809. https://doi.org/10.1016/j.conbuildmat.2020.118809

Petersen, J. C. (2009). A review of the fundamentals of asphalt oxidation: Chemical, physicochemical, physical property, and durability relationships. *Transportation Research Circular (E-C140)*.

Pipintakos, G., Sreeram, A., Mirwald, J., & Bhasin, A. (2024). Engineering bitumen for future asphalt pavements: A review of chemistry, structure and rheology. *Materials & Design*, *244*, 113157. https://doi.org/10.1016/j.matdes.2024.113157

Read, J., & Whiteoak, D. (2003). *The shell bitumen handbook*. Thomas Telford.

Sakib, N., & Bhasin, A. (2019). Measuring polarity-based distributions (sara) of bitumen using simplified chromatographic techniques. *International Journal of Pavement Engineering*, *20*(12), 1371–1384. https://doi.org/10.1080/10298436.2018.1428972

Schwettmann, K., Höhne, P., & Stephan, D. (2022). Comparison of column chromatography and solid-phase extraction on virgin and aged bituminous maltene phases. *Materials and Structures*, *55*(10), 242. https://doi.org/10.1617/s11527-022-02079-4

Shi, H., Xu, T., Zhou, P., & Jiang, R. (2017). Combustion properties of saturates, aromatics, resins, and asphaltenes in asphalt binder. *Construction and Building Materials*, *136*, 515–523. https://doi.org/10.1016/j.conbuildmat.2017.01.064

Wang, J., Wang, T., Hou, X., & Xiao, F. (2019). Modelling of rheological and chemical properties of asphalt binder considering sara fraction. *Fuel*, *238*, 320–330. https://doi.org/10.1016/j.fuel.2018.10.126